

# AEROELASTICITY OF A LAMINAR WING

**Holger Mai<sup>1</sup>, Anne Hebler<sup>2</sup>**

<sup>1</sup> Team Leader

Institute of Aeroelasticity of the German Aerospace Center (DLR)  
Bunsenstr. 10, 37073 Goettingen, Germany  
holger.mai@dlr.de

<sup>2</sup> Engineer

Institute of Aeroelasticity of the German Aerospace Center (DLR)  
Bunsenstr. 10, 37073 Goettingen, Germany  
anne.hebler@dlr.de

**Keywords:** laminar wing, transition, aeroelasticity, flutter stability.

**Abstract:** Within the DLR Institute of Aeroelasticity project iGREEN (integrated green aircraft) the aeroelastic behavior of a typical laminar airfoil under unsteady transonic flow conditions was to be investigated. For that a 2D airfoil model was build and tested in the transonic wind tunnel facility DNW-TWG in Goettingen. The model is a 2D-section with a CAST-10 profile, made of carbon reinforced fiber (CRF). It is equipped with 60 unsteady pressure sensors placed in one section and with hot-film sensors located on its upper and lower surface between 10% and 85% in steps of 5% in streamwise direction, 16 on each side. In order to get a smooth surface without disturbing the laminar flow, the hot-film foil is embedded in the model. In the steady case the upper surface of the model was observed with two infrared cameras. The model was installed in the institutes 2D test set-up for forced pitch oscillations. Under harmonic pitch oscillations the time dependent pressure distribution, global forces and the variation of the transition region were measured for three different flow conditions (subsonic, weak transonic and transonic with strong shock and possible separation).

The results may lead to a physical understanding of the interaction of unsteady transition and shock position and act as validation data for new unsteady transition prediction models.

## 1 INTRODUCTION

Within its vision 2020 the Advisory Council for Aeronautic Research in Europe (ACARE) proclaimed a target of reduction of fuel consumption and CO<sub>2</sub> emissions by 50% and NO<sub>x</sub> reduction by 80%. For modern transport aircraft operating in the transonic regime, drag reduction is expected to have the highest potential contributing to these aims. The potential of drag reduction on the whole aircraft by laminar flow on the wing is estimated by 11%. However, the influence of the integration of such a new technique, which may change flow characteristics significantly in contrast to modern supercritical transport aircraft wing profiles, on the aeroelastic behavior is totally unknown. Because of the altered shape of laminar wings, the supersonic region is larger and therefore shock strength and dynamics may increase (see Figure 1).

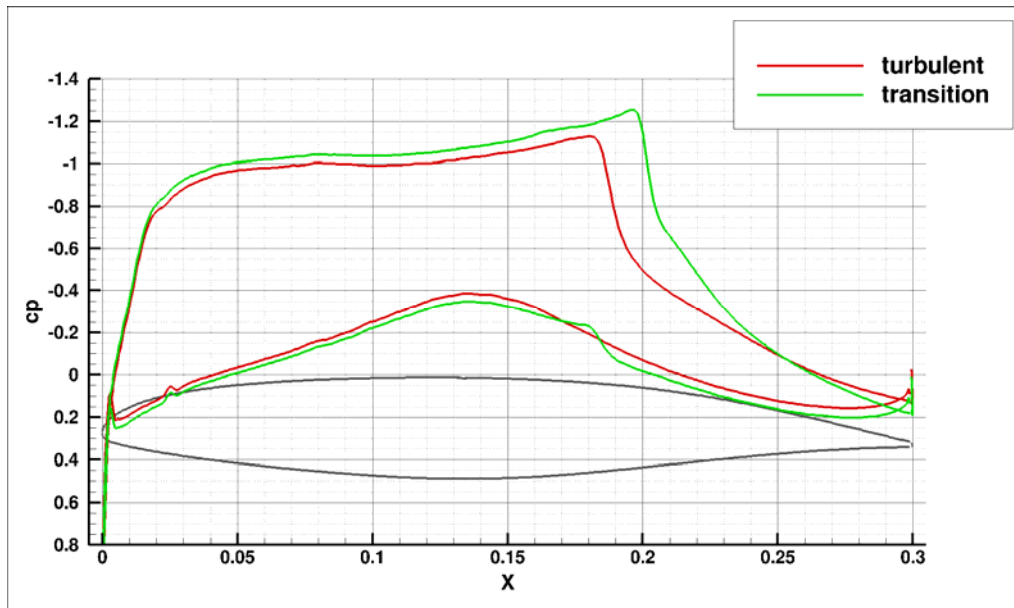


**Figure 1:** Pressure distribution for the CAST-10 profile with laminar and fully turbulent flow condition ( $Ma=0.765$ ,  $Re=2e06$ ,  $\alpha=2^\circ$ ). Calculated with DLR Tau code by G. Voß.

Our former investigation [1], [2] showed that exactly these phenomena are of great importance for aeroelastic stability and flutter. It may be expected that the so called transonic dip is more pronounced and buffeting already occurs at smaller transonic mach numbers.

To clarify this, the processes that take place in the unsteady boundary layer of an oscillating airfoil have to be described in more detail. A good indicator for the activities in the boundary layer is the wall shear stress, as it changes for the different flow states. Experimentally the wall shear stress can be determined using hot wire anemometry or hot-film sensors. Lee and Basu [3] as well as Lee and Gerontakos [4] used multiple hot-film sensor arrays to analyze the flow around a NACA0012 airfoil. They described the movements of the leading-edge stagnation point, flow separation and reattachment points, boundary layer transition and relaminarization and flow reversal in low-speed flow. Another technique to determine the laminar-to-turbulent transition was applied by Studer et al. [5], who used hot wire anemometry to evaluate the mode of transition. They were able to detect the convective and creative mode applying a wavelet-skewness-method. Their measurements were conducted at low-speed conditions with the model held in a fixed position and the flow oscillating. The behavior of the boundary layer in transonic flow and the interaction with the shock has been examined for static cases by Swoboda and Nitsche [6]. In order to investigate the behavior of the boundary layer on an oscillating profile in transonic flow, hot-film sensors were applied in this study, as they are non-intrusive and oscillate with the model.

A systematic aeroelastic investigation for laminar wings is unknown in the literature. Numerical prediction tools for unsteady transition are still under development [7]. Therefore we started an investigation on the interaction of the laminar-turbulent transition with a shock under unsteady transonic flow conditions.

## 2 EXPERIMENT

### 2.1 Wind tunnel model and instrumentation

First a suitable profile that exhibits significant laminar flow run length had to be found. The main constraint is that only Reynolds numbers of 1-6mio. are possible in the designated wind tunnel DNW-TWG. Modern designed profiles are usually made for higher Reynolds numbers, but as our objective was the basic investigation of the physical phenomena of a shock and transition any laminar profile would be suitable. We chose the Dornier CAST-10 profile, which was object of several investigations by DLR and NASA already [8].

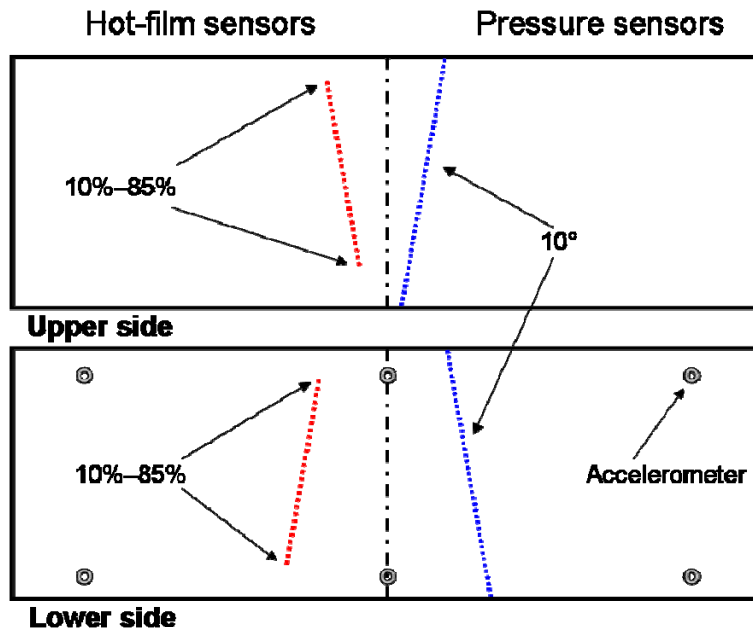


Figure 2: Sensor distribution on the CAST-10 profile

As the main objective of this investigation was the measurement of the unsteady motion of the laminar-turbulent transition, it was decided to equip the wind-tunnel model with unsteady pressure sensors, hot-film sensors and accelerometers. The accelerometers are used to measure the motion of the oscillating profile, the unsteady pressure sensors are used to measure the pressure distribution in one representative section and the hot-film sensors are used to measure the condition of the boundary layer. A schematic diagram of the arrangement of the sensors at the model can be found in Figure 2.

The hot-film sensors work by the principle that a small resistor is heated and controlled to a constant resistance. When the sensor element is cooled by the air flow the resistance changes and the current has to be adjusted by the controller electronics. As the sensor element itself is held very small, it can react very fast to changes of the flow velocity. The sensor elements in our case are 1.45mm long, 0.1mm wide and 0.2 $\mu$ m high. They are made of nickel that is sputtered on a Kapton foil of 50 $\mu$ m thickness. The connecting leads to each sensor element were thickened by copper to 3.8 $\mu$ m to increase conductivity. The sensor foil was manufactured by TAO Systems, U.S.A. We chose a number of 16 sensor elements on the upper and lower side of the model with a spacing of 5% between 10% and 85% chord length in stream wise direction. The sensor elements on each foil are arranged with an angle of 10 degrees to prevent add up of disturbances. For the application of the foil on the model surface, a pocket of slightly larger dimensions and of exact depth of the thickness of the foil and adhesive film was laminated into the surface. The hot-film foil was then glued in and the gap was filled and polished.

Usually connecting wires are soldered to the hot-film foil and fed outside of the wind tunnel on the surface of the model. To prevent these disturbances of the laminar flow, we connected the sensors to the inside of the model by connecting pins through the surface of the laminate. Soldered to the pins are miniature coax cables that conduct the electric signal to the outside of the model and from there over a total distance of 10m to the anemometer amplifiers. Sensors and electronics are capable of resolving fluctuations up to 60kHz. During the installation in the wind tunnel, two sensors from the upper side of the airfoil, located at 35% and 50% of the chord, were damaged and could not be used.

The model is equipped with 60 unsteady pressure sensors of type Kulite XCQ-093D in one section. The pressure tabs are also arranged in one line with an angle of 10 degrees like the hot-film sensors.

Between the pressure tabs and the hot-film foil an area of 20mm in the exact mid span section is left blank to have a clean area where we measured the drag very accurately with a wake rake. This was done to have a very accurate measure for comparison with numerical simulations in the future.

Six accelerometers of type PCB 352C22 were installed at  $y/l=15\%$  50% and 85% span wise direction and  $x/c = 8.33\%$  and 87.33% chord length.

## 2.2 Test set-up

The model was mounted to a hydraulic pitch-oscillation test set-up, which is arranged symmetrically outside of each wind tunnel test-section side wall. Figure 3 shows a sketch of this pitch-oscillation test set-up.

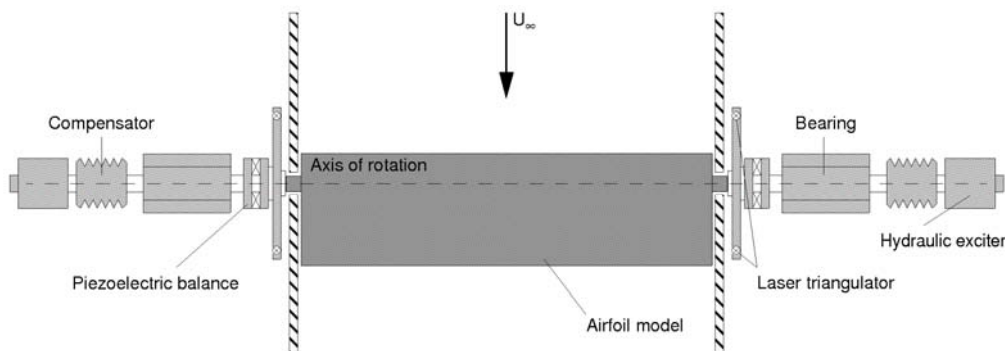


**Figure 3:** Arrangement of set-up for forced pitch oscillations of the CAST-10 model in the wind tunnel.

The angle of attack of the symmetrically installed model can be varied by  $\pm 10^\circ$  via two hydraulic exciters operated in phase opposition. Forced pitching oscillations with maximum amplitude are possible only at small frequencies. Up to a frequency of 50Hz the possible amplitude decreases to  $1^\circ$ .

The suspension system comprises a compensator, a bearing and a piezoelectric balance. This balance consists of four three-component piezoelectric elements of type Kistler 9047B and 9048B, which are mounted by pre-stressed bolts between two plates. Each element can measure forces in x-, y- and z-direction. In combination of all four elements lift, drag and pitching moment can be measured. The piezoelectric balance is described in detail in [9].

Close to the model is a bar acting as a reference for laser triangulators. By these, the instantaneous angle of attack of the model can be measured by triangulation.

For the whole test we defined a right hand coordinate system that originates at the right wind tunnel wall (looking downstream) at the leading edge of the CAST-10 model at 50% wind tunnel height. X-direction is downstream, y-direction is in span-wise direction and z-direction is positive in positive lift direction.

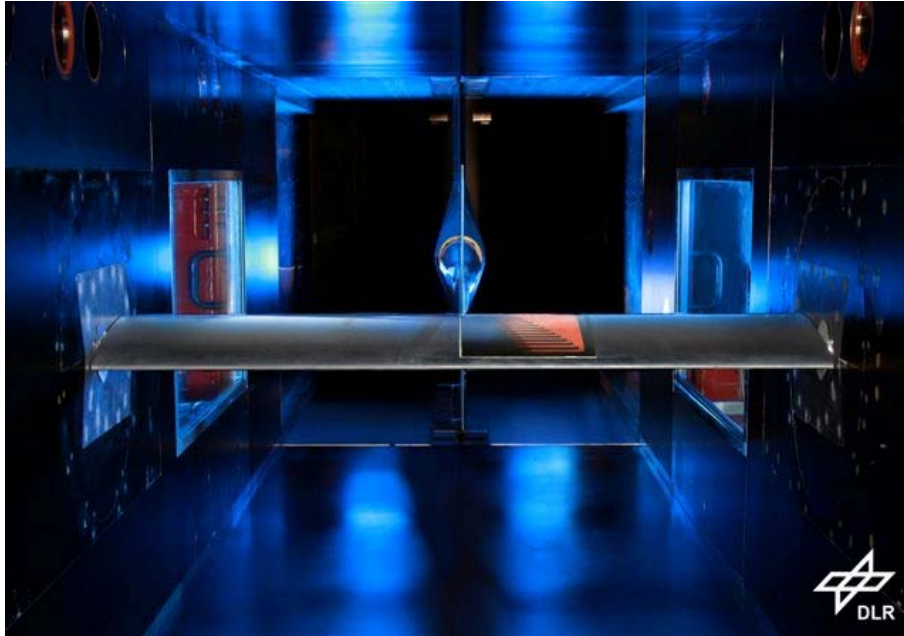


**Figure 4:** Downstream view on the upper surface of the CAST-10 model in the adaptive test section of the DNW-TWG wind tunnel.

### 2.3 Data Acquisition System

All unsteady signals were recorded with a data acquisition system that encompasses a 24bit Delta-Sigma A/D converter for each channel. The system is capable of acquiring data with a maximum sample rate of 204.8kHz per channel. 32 channels of unsteady pressures from the wind tunnel top and bottom walls, 60 channels of unsteady pressures from the CAST-10 model, 6 accelerometer signals, 4 balance signals and 4 laser triangulators were sampled at variable sample rate of 128 times the model oscillation frequency. 32 unsteady signals from the hot-film sensors were sampled at a fixed sample rate of 120kHz.

Steady mean data from the wind tunnel, like total pressure, static pressure, static temperature, Mach number, steady wall pressures and adaptive wall position are transferred by file to the data acquisition system and saved together with the unsteady data.

### 2.4 Wind tunnel

The tests were performed in the Transonic Wind Tunnel Goettingen (TWG), operated by the foundation German-Dutch Wind Tunnels (DNW). This is a continuous run facility with a 1m x 1m adaptive test-section. The top and bottom walls of the test section are adapted to the steady flow around the wind tunnel model. The residual wall interference is minimized by a one step method of wall adaptation based on a Cauchy type integral [10] using the top and bottom wall static pressure distributions. The accuracy of the wall pressures is estimated to be  $\pm 0.35\%$  with respect to the test stagnation pressure. The displacement thickness of the turbulent wind tunnel wall boundary layer is predicted by Head's method [11] and is added to the wall shapes; top and bottom wall displacement thicknesses are obtained according to the measured pressure gradients at each wall, while the gradient is neglected for the sidewalls [12]. During the dynamic tests, the wind tunnel walls were adapted to the steady flow at each mean incidence of the model which was chosen for the following oscillation tests. It was shown in a previous investigation [13] that this minimizes wind tunnel wall interference effects also during the oscillation tests. The DNW-TWG has the advantage that it covers the whole speed range from  $Ma=0.300$  to  $Ma=0.850$  using the adaptive test section.

For a reference chord length of  $c=0.3\text{m}$  the possible Reynolds number is between  $Re=0.5$  Mio. and  $Re=6$  Mio. In Figure 5 the whole wind tunnel is depicted schematically.

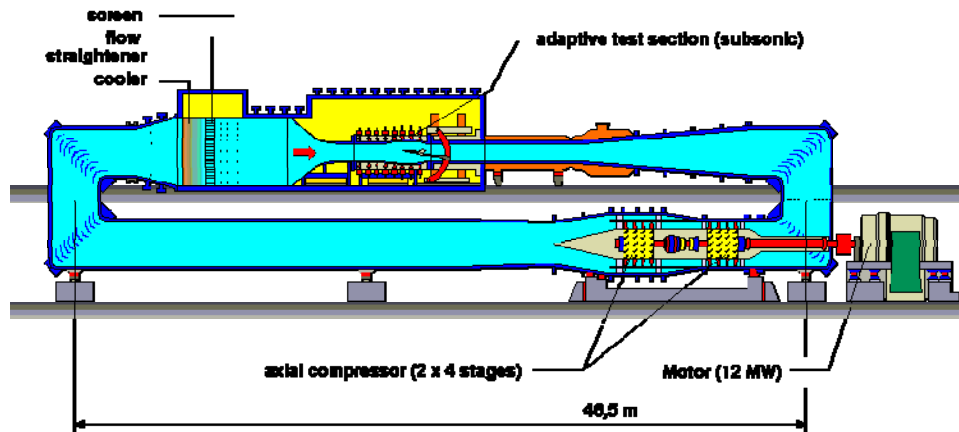


Figure 5: Transonic Wind Tunnel Goettingen (DNW-TWG).

## 2.5 Test program

All test points in the program were measured with the clean wing with free transition and with fixed transition. For the latter transition dots of 0.127mm height were glued on the upper model surface at 17.5% chord length and of 0.0787mm height on the lower surface at 7.5% chord length.

We selected four Mach numbers: one subsonic Mach number without shock ( $Ma=0.500$ ), one moderately transonic Mach number where we expected shock motion ( $Ma=0.700$ ), one Mach number close to the design point of the airfoil with shock motion ( $Ma=0.765$ ) and one Mach number where we expected already a strong fixed shock and separation ( $Ma=0.800$ ). For all Mach numbers steady polars were measured to characterize the steady flow field. Afterwards we measured unsteady test cases with amplitude variations at three different reduced frequencies between  $0.05 \leq \omega^* \leq 0.40$ .

## 3 RESULTS

### 3.1 Steady results

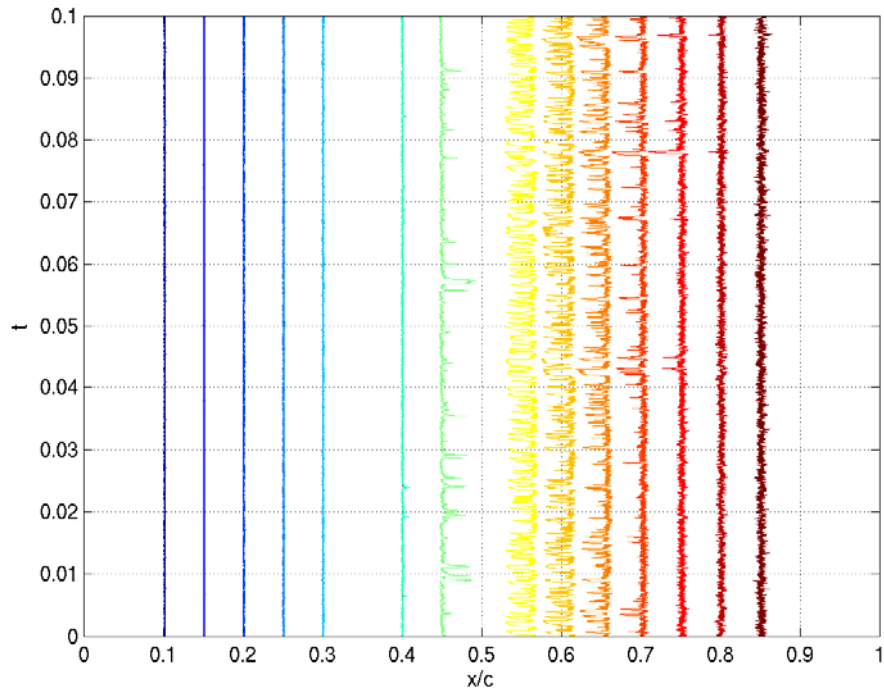
#### 3.1.1 Hot-film measurements

Figure 6 shows the time series of the signals, measured by the hot-film sensors located on the upper side of the profile for  $Ma=0.500$  and  $\alpha_0=-0.6$ . As these sensors were not calibrated, and hence the absolute values do not provide any information, the mean value of each signal is subtracted and the signals are shifted to their corresponding position in x-direction.

The sensors located between 10% and 30% of the chord show only little fluctuations, here the flow is laminar. The development of the state of the boundary layer can additionally be observed using the statistical values standard deviation and skewness of the signal, shown in Figure 7 for the same case. While the flow is laminar, the fluctuations of the wall shear stress are small and the measured values are normally distributed so that the standard deviation is small and the skewness is nearly zero.

The transitional region is subdivided into 3 parts. The first one is dominated by laminar flow, but turbulent peaks are present. This causes the standard deviation to grow and the skewness to become positive. Starting from 40% chord turbulent spots are growing in the laminar boundary layer passing into immense fluctuations, which cover the sensors at 55% and 60% chord. There the signals jump between the levels of laminar and turbulent flow,

which means that an intermittency of 50% is reached. The standard deviation reaches its maximum and the skewness becomes zero again. But in this case the values are not normally distributed around a mean, rather there are two peaks in the distribution. The third part is governed by turbulent flow with the presence of laminar peaks, resulting in a negative skewness. This can be seen at the sensors positioned between 65% and 75% chord. Downstream of the sensor at 80% chord the flow is fully turbulent. Here, the skewness becomes zero again, with a normal distribution. The standard deviation is reduced, but still on a higher level than it was for laminar flow.



**Figure 6:** Time series of the hot-film signals on the airfoil's upper surface. ( $Ma = 0.500$ ,  $\alpha_0 = -0.64^\circ$ )

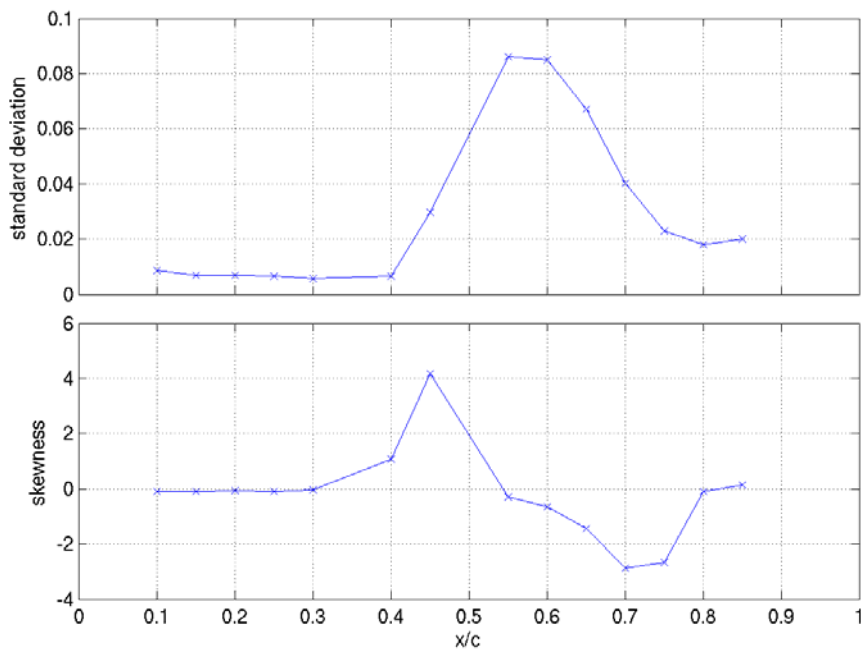


**Figure 7:** Statistical evaluation of the hot-film signals on the airfoil's upper surface. ( $Ma = 0.500$ ,  $\alpha_0 = -0.64^\circ$ )

A static polar was recorded for angles of attack between  $-1^\circ \leq \alpha_0 \leq +4^\circ$  at  $Ma=0.500$ . The results of the hot-film measurements were analyzed as described before and plotted in Figure 8. The color of the bars indicate the state of the boundary layer, green for laminar flow, blue for turbulent flow and cyan for the transitional region. It can be seen that the transition moves upstream while increasing the angle of attack. At the same time a decrease of the spatial expansion of the transitional region can be noticed.

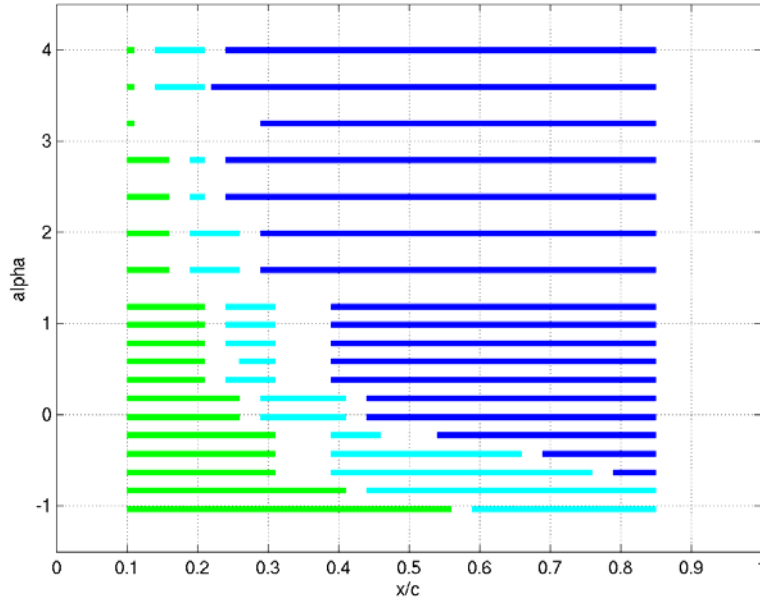


**Figure 8:** State of the flow at  $Ma=0.500$  (green: laminar, cyan: transitional, blue: turbulent)

Plotting the same for the polar at  $Ma=0.700$ , a different behavior of the transition movement occurs (Figure 9). The transition moves upstream up to an angle of attack of  $\alpha_0=1^\circ$ , but then it moves downstream. To clarify this unexpected behavior, the results of the pressure measurements were looked at. Starting at an angle of attack of  $\alpha_0=0.8^\circ$  a shock develops on the upper side of the airfoil at 20% of the chord, moving downstream with increasing angle of attack up to 45% chord at  $\alpha_0=4^\circ$ . A laminar separation bubble occurs, which can be seen in the pressure measurements as well as in the hot-film measurements.

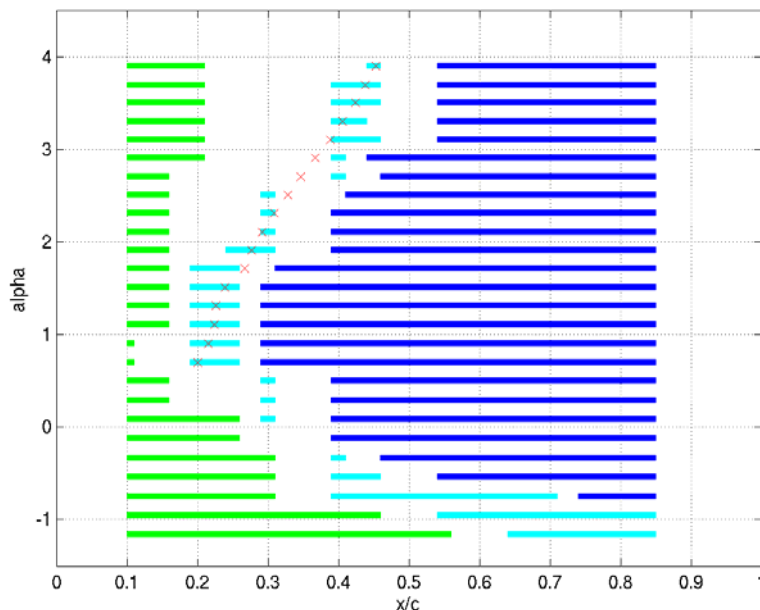


**Figure 9:** State of the flow at  $Ma=0.700$  (green: laminar, cyan: transitional, blue: turbulent, x: shock position)

### 3.1.2 Infrared measurements

The hot-film sensors gave us the possibility to observe the variation of the laminar-turbulent transition very fast but only for one section. In order to have the possibility to verify this at least in the steady case and also to observe 3D effects in the transition, like transition as a result of imperfections or damages in the model surface, two infrared cameras were used to observe the flow above the models upper surface. The working principle is based on the Reynolds analogy, since the heat transfer into the aerodynamic surface is proportional to the wall shear stress. The wall shear stress of a turbulent boundary layer is much larger than that of a laminar boundary layer, and the wall shear stress at the separation line is zero. These differences in the wall shear stress come along with differences in the heat transfer between the flow and the model structure. By an initial temperature difference between the wind-tunnel model and its ambience, the locally different heat transfer will cause a non-uniform temperature distribution on the model surface which will radiate into the infrared spectrum. Thus, the wall shear stress distribution can be visualized by an ordinary thermographic infrared camera. For every steady data point, one image was captured with each infrared camera.

In Figure 10 infrared images for a test case at  $Ma=0.700$  and an angle of attack of  $\alpha_0=1.2^\circ$  are shown. Bright dots are the hot-film sensors. It can be seen that transition takes place along a more or less uniformly line at 23% chord (between third and fourth hot-film sensor) which is consistent with the results shown in Figure 9. We do not find any hint for premature transition due to roughness at the model nose or due to different surface roughness on the model and the hot-film foil. This was the case some days later during the test, when roughening occurred especially on the flexible hot-film foil by impacts of very small particles. At that time the test with laminar flow was finished and transition dots were glued on the model for the test points with fixed transition anyway.

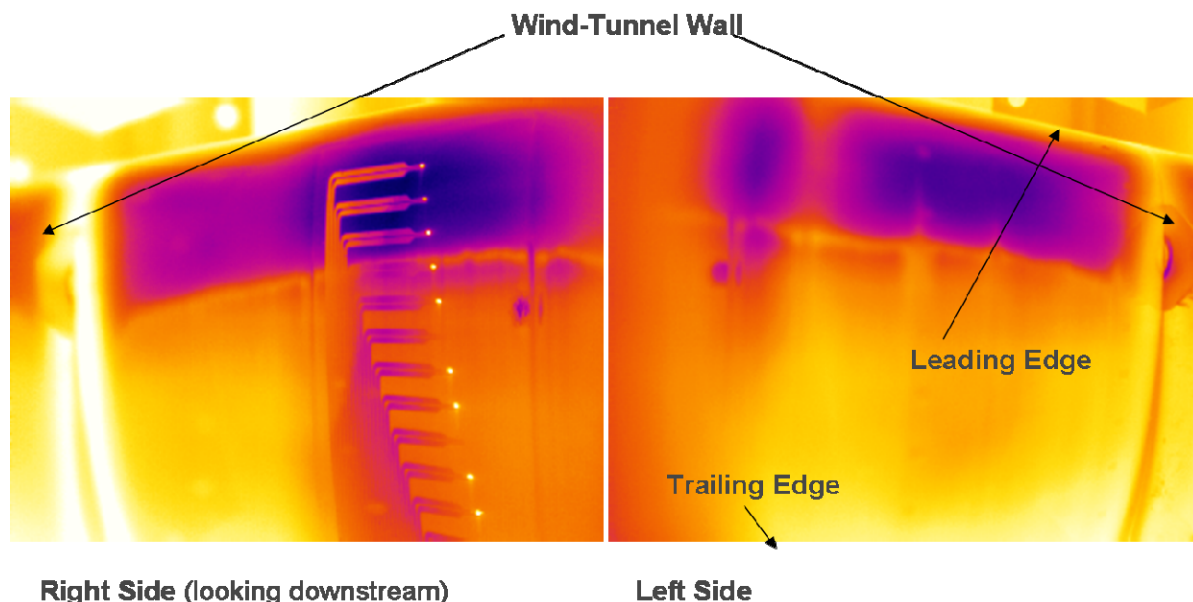


**Figure 10:** Infrared measurements of model suction side for a test case of  $Ma=0.700$  and  $\alpha_0=1.2^\circ$ .

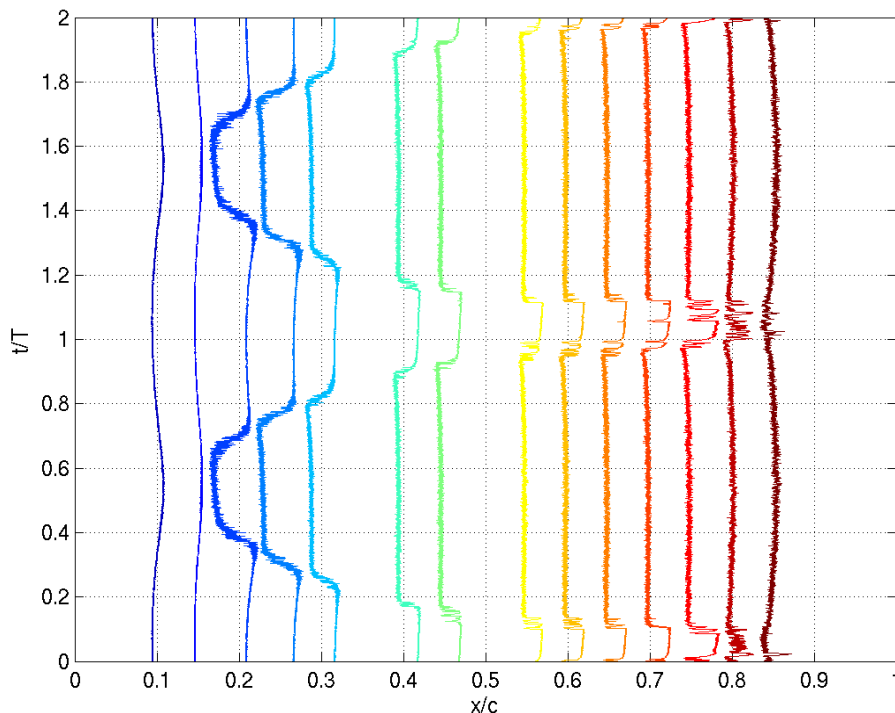
## 3.2 Unsteady results

### 3.2.1 Hot-film measurements

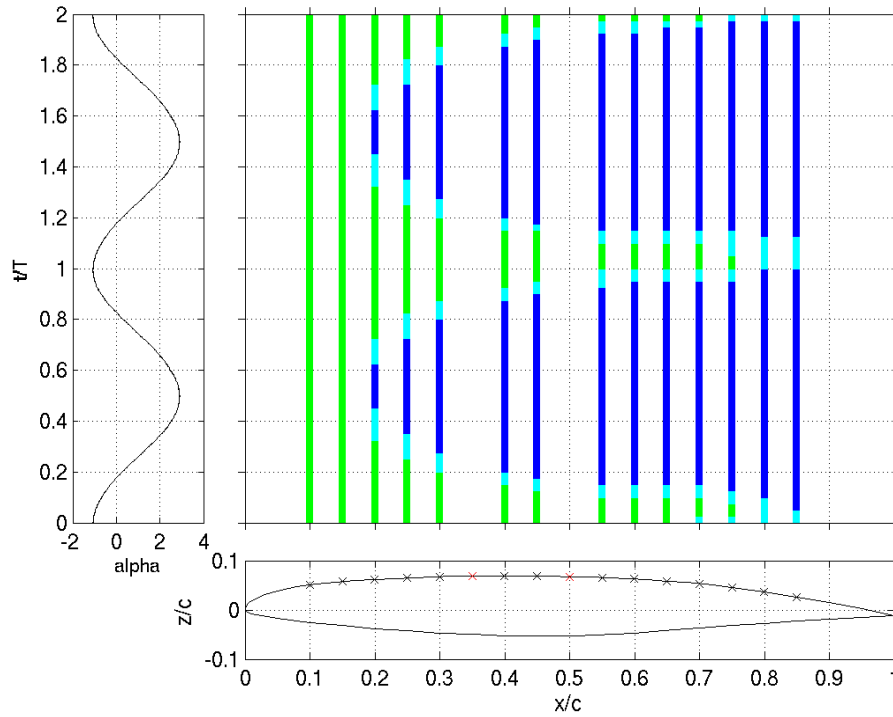
Unsteady measurements were carried out for the same Mach numbers as for the steady measurements for varying reduced frequencies and amplitudes.

Figure 11 shows the time series of the upper side sensors for two periods during an oscillation of  $\alpha = 0.91^\circ \pm 2.0^\circ$  at  $Ma=0.500$ . Again, the mean value of each sensor was subtracted. Starting at the sensor at  $x/c=0.2$ , the signals swap between two distinct levels during one period. For the lower level, the heat transfer is small which indicates low shear stress and therefore laminar flow. Likewise, the higher output level of the voltage represents high heat transfer, thus turbulent flow. Hence, the rise and the fall between the two levels indicate transition and relaminarization above the sensor, respectively. The evaluation of the hot-film signals for the same case is shown in Figure 12. The transition movement covers a region of about 70% of the chord during an oscillation with an amplitude of  $\Delta\alpha=2^\circ$  around a mean angle of attack of  $\alpha_0=1^\circ$ . It reduces to 5% to 10 % chord when the airfoil oscillates with an amplitude of  $\Delta\alpha=0.2^\circ$ .

The results shown in Figure 13 were recorded at  $Ma=0.700$  and  $\alpha = 0.83^\circ \pm 0.99^\circ$ . The transition moves between  $x/c=0.25$  and  $x/c=0.3$ . It can be seen that the flow changes from laminar to turbulent and back twice within one period. This matches with the results of the static cases, where it was shown that the transition moves upstream up to an angle of attack of  $\alpha_0=1^\circ$  followed by downstream movement.



**Figure 11:** Time series of the hot-film signals on the airfoil's upper surface. ( $Ma = 0.500$ ,  $\alpha_0 = 0.91^\circ \pm 2.0^\circ$ )



**Figure 12:** Top left: model oscillation, top right: state of the flow at  $Ma=0.500$  (green: laminar, cyan: transitional, blue: turbulent), bottom: airfoil profile with sensor positions (damaged sensors marked by red x)

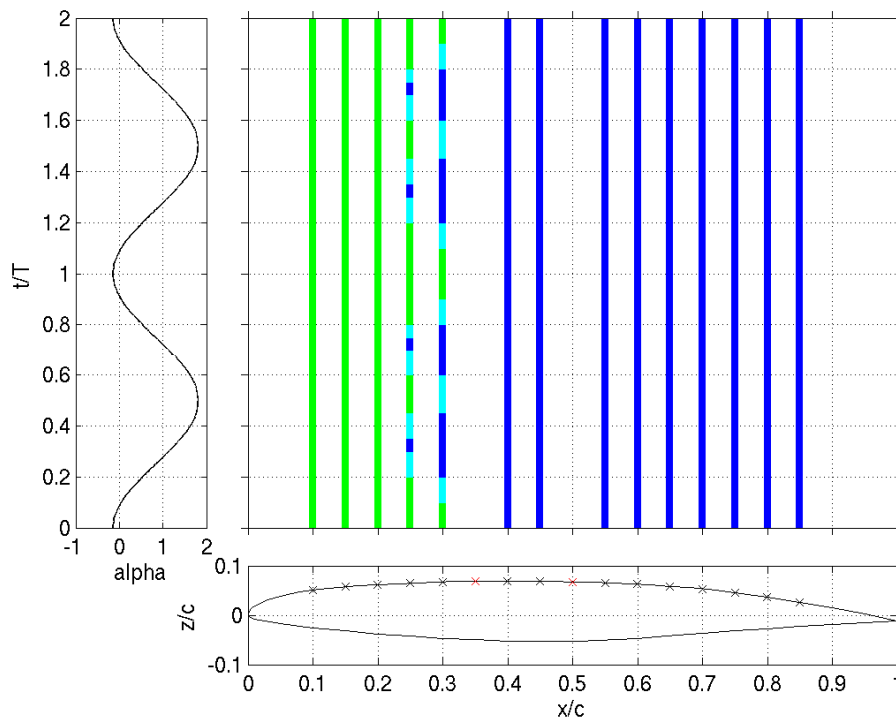


**Figure 13:** Top left: model oscillation, top right: state of the flow at  $Ma=0.700$  (green: laminar, cyan: transitional, blue: turbulent), bottom: airfoil profile with sensor positions (damaged sensors marked by red x)

### 3.2.2 Pressure measurements

From the 60 pressure sensors we integrated the local lift and moment coefficients. In Figure 14 we show the lift and moment slopes for oscillations at each of the four Mach numbers for

the lowest reduced frequency  $\omega^*=0.05$ . At  $Ma=0.500$  and  $Ma=0.700$  we intended an oscillation with an amplitude of  $\Delta\alpha=1^\circ$  around a mean angle of attack of  $\alpha_0=1.0^\circ$ . At the higher Mach numbers it was not possible to go to such high angles and we performed smaller oscillations around  $\alpha_0=0.0^\circ$ . Due to later corrections the real angles and amplitudes differ from the target values.

At  $Ma=0.500$  we see an almost linear behavior of the coefficients for transitional and turbulent flow. At  $Ma=0.700$  it is nearly the same but above  $\alpha_0=1.4^\circ$  a shock occurs that may induce small nonlinearities in the slopes.

At  $Ma=0.765$  it is very impressive to see that in the turbulent case lift and moment are still linear but for the transitional flow we observe strong nonlinearities. Finally at  $Ma=0.800$  we see nonlinear behavior already in the turbulent case.

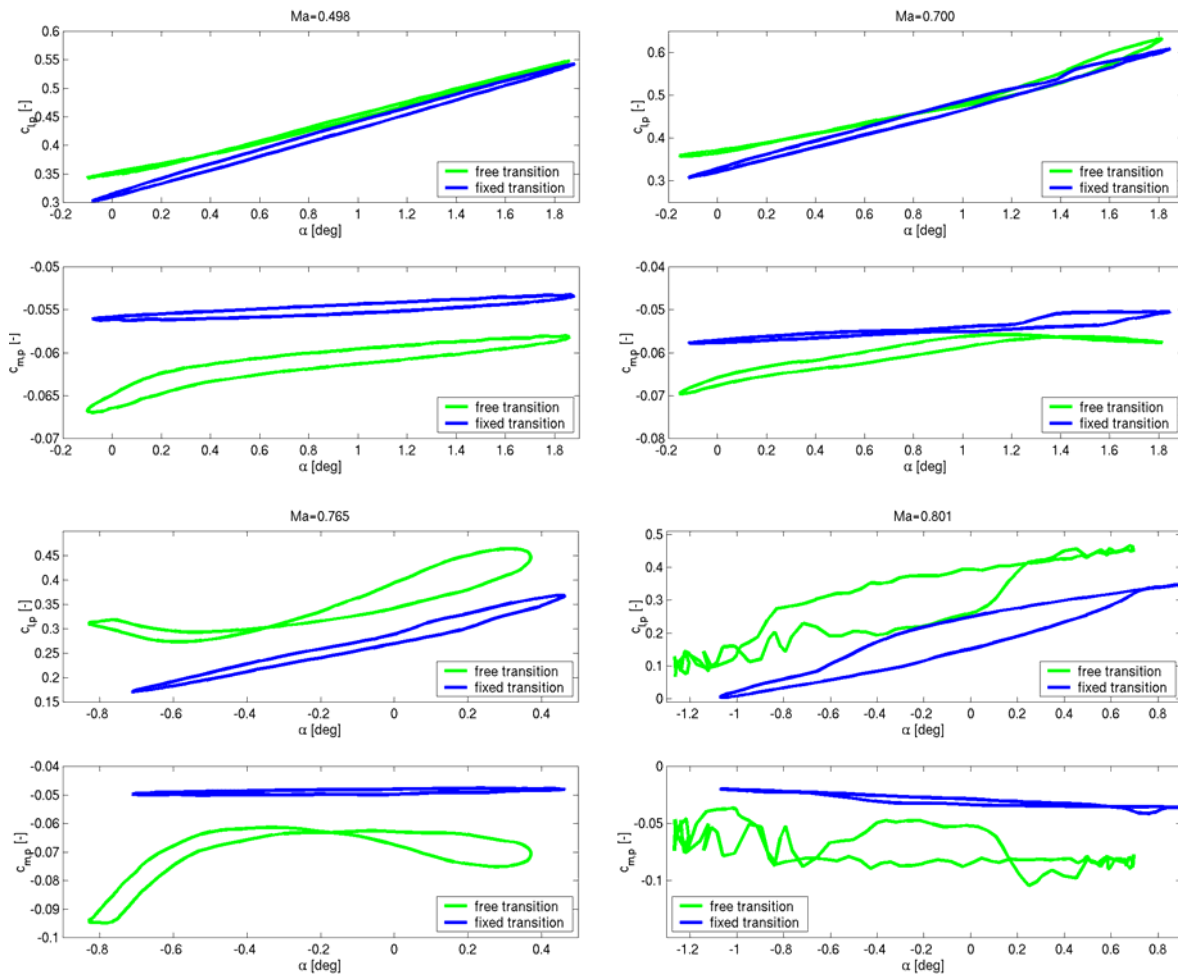


**Figure 14:** Unsteady lift and moment coefficients for oscillations with a reduced frequency of  $\omega^*=0.05$  for four different Mach numbers: Top left:  $Ma=0.500$ , top right:  $Ma=0.700$ , lower left:  $Ma=0.765$ , lower right:  $Ma=0.800$ .

#### 4 SUMMARY AND CONCLUSIONS

In the DNW-TWG transonic wind tunnel facility Goettingen we investigated the unsteady behavior of the laminar-turbulent boundary transition of an oscillating CAST-10 airfoil model. For that the model was equipped with hot-film sensors, unsteady pressure sensors and accelerometers. Laminar-turbulent transition takes place at different chord positions depending on Mach number and angle of attack. Remarkably, transition does not take place at a fixed chordwise position but shows a more or less large area with intermittent state of

the boundary layer. This can be resolved quite well with the chosen discretisation of the hot-film sensors of 5% chord. At Mach numbers higher than  $Ma=0.700$  the sensor spacing is too coarse and transition takes place between two sensors. Therefore up to now no direct correlation of the motion of the shock and the variation of the transition region is possible. In order to resolve this better, a new hot-film foil with a larger number of sensors or adapted spacing will have to be manufactured. Nevertheless it should be emphasized that actual transition models like the  $e^N$  method use only one factor to describe the progress of transition, which may be insufficient for a process that takes place over up to half of the chord length.

From the integrated lift and moment coefficients we see that with the occurrence of shocks in the transonic flow strong nonlinearities in the transitional flow occur, whereas in the fully turbulent case it is still linear. Even if we do not have direct measurements of the stability limits, it can be assumed that these nonlinearities will influence the stability at transonic air speeds. In a follow up test this stability limit will be measured directly in a flutter test.

## 5 ACKNOWLEDGEMENTS

This work was funded by DLR programmatic research in a project called “iGREEN”. The hot-film measurements were conducted in cooperation with Dr. G. Hoehler and Dr. S. Koch. The infrared measurements were performed by Dr. K. deGroot. The authors would like to thank for the good and valuable cooperation. We would further like to thank Mr. J. Berold and Mr. H. Boehlken for thorough preparation of the wind tunnel model, Mr. Th. Buete being responsible for the operation of the test set-up, Mr. J. Nuhn for thorough preparation and conduction of the test and acquisition of the data, and the team of the DNW-TWG for their support and operation of the wind tunnel.

## 6 REFERENCES

- [1] DIETZ G., SCHEWE G., MAI H., *Experiments on Heave/Pitch Limit-Cycle Oscillations of a Supercritical Airfoil close to the Transonic Dip*, Journal of Fluids and Structures 19, 1-16, 2004.
- [2] DIETZ, G., SCHEWE G., MAI H., *Amplification and Amplitude Limitation of Heave/Pitch Limit-Cycle Oscillations Close to the Transonic Dip*, Journal of Fluids and Structures 22, 505-527, 2006.
- [3] LEE T., BASU S., *Measurement of unsteady boundary layer developed on an oscillating airfoil using multiple hot-film sensors*, Experiments in Fluids 25, 108-117, 1998.
- [4] LEE T., GERONTAKOS P., *Investigation of flow over an oscillating airfoil*, J. Fluid Mech. , vol. 512, pp. 313–341, 2004.
- [5] STUDER G., ARNAL D., HOUEVILLE R., SERAUDIE A.: *Laminar-turbulent transition in oscillating boundary layer: experimental and numerical analysis using continuous wavelet transform*, Experiments in Fluids, 41:685–698, 2006.
- [6] SWOBODA M., NITSCHKE W.: *Shock Boundary-Layer Interaction on Transonic Airfoils for Laminar and Turbulent Flow*, Journal of Aircraft, Vol. 33, No. 1, January-February 1996.
- [7] KRUMBEIN A., KRIMMELBEIN N., SCHRAUF G., *Automatic Transition Prediction for Three-Dimensional Aircraft Configurations using the DLR TAU Code*. In: Notes on Numerical Fluid Mechanics and Multidisciplinary Design New Results in

Numerical and Experimental Fluid Mechanics VII, Vol. 112. Springer Verlag, Berlin, Heidelberg . pp. 101-108. ISBN 978-3-642-14242-0. ISSN 1612-2909, 2010.

[8] STANEWSKY E., DEMURIE F., RAY E.J., JOHNSON C.B., *High Reynolds number tests of the CAST-10-2/DOA 2 transonic airfoil at ambient and cryogenic temperature conditions*, AGARD-CP-348, pp. 10-1 – 10.13, 1984.

[9] SCHEWE G., *Force measurements in aeroelasticity using piezoelectric multicomponent transducers*, International Forum on Aeroelasticity and Structural Dynamics, Aachen, June 3–6, DGLR Report 91-06, 1991.

[10] WEDEMEYER E., TAYLOR N. J., HOLST H., *Adaptive Wall Techniques*, AG 336, AGARD, 1998.

[11] CEBECI T., BRADSHAW P., *Momentum Transfer in Boundary Layers*, McGraw-Hill, New York, 1979.

[12] JACOBS M., Treatment of the Wall Boundary Layer in the Wall Adaptation Procedure and Steady Wall Adaptation for Dynamic Tests, private communication, DNW BU GuK, Goettingen, 2002.

[13] GEIBLER W., DIETZ G., MAI H., *Dynamic Stall on a Supercritical Airfoil*, 29th European Rotorcraft Forum, 16.–18. September 2003, Friedrichshafen, Germany, 2003.